

Quantum thermodynamic processes: A control theory for machine cycles

Jan Birjukov^{1,a}, Thomas Jahnke², and Günter Mahler²

¹ Chair for Theoretical Physics and Applied Mathematics, Urals State Technical University, Mira 19, 620002 Jekaterinburg, Russia

² Institut für Theoretische Physik 1, Universität Stuttgart, Pfaffenwaldring 57, D-70550 Stuttgart, Germany

Received: 8 November, 2007 / Revised version: 20 May, 2008

Abstract. The minimal set of thermodynamic control parameters consists of a statistical (thermal) and a mechanical one. These suffice to introduce all the pertinent thermodynamic variables; thermodynamic processes can then be defined as paths on this 2-dimensional control plane. Putting aside coherence we show that for a large class of quantum objects with discrete spectra and for the cycles considered the Carnot efficiency applies as a universal upper bound. In the dynamic (finite time) regime renormalized thermodynamic variables allow to include non-equilibrium phenomena in a systematic way. The machine function ceases to exist in the large speed limit; the way, in which this limit is reached, depends on the type of cycle considered.

PACS. 05.30.-d Quantum statistical mechanics – 05.70.Ln Nonequilibrium and irreversible thermodynamics

1 Introduction

Thermodynamics [1,2,3] has long since been supposed to be an extremely efficient phenomenological theory, though with regard to large systems only. However, it has recently been shown that thermodynamical properties emerge already for small quantum systems provided they are embedded in some appropriate environment [4]. As a consequence, the idea that a single quantum object might well be described by means of thermodynamic concepts should no longer be considered self-contradictory. Nanothermodynamics [5,6] is becoming an emergent field that might be relevant to many areas ranging from nano-physics to molecular biology.

Among the basic concepts of thermodynamics there are two standing out for their fundamental and practical significance: heat and work. It is not surprising that issues concerning quantum thermodynamic machines attract so much theoretical interest [7,8,9,11,12,13,14,15,16,17].

Various possible levels of description can mainly be classified by the extent to which explicit quantum effects are being taken into account. So, time dependence may either be included by means of a classical driving system or by coupling to another full quantum mechanical subsystem [17]. The dynamics of the machine may or may not be allowed to manifest some quantum mechanical coherence. Anyway, in this context one should observe that the coupling to heat baths is not an unavoidable nuisance, but

an essential part of the operation of any thermodynamic machine; decoherence [18] should thus be dominant.

In this paper we intend to explore the universal limitations for the performance of a quantum thermodynamic machine as it arises from a conceivable driving scheme and those quantum properties of the working substance, which could survive strong decoherence: the discrete spectrum and probabilistic character of the state. For this purpose we employ a kind of control theory approach with two formal parameters, one related to the spectrum and another to the state of a quantum system (cf. [8,9,10]). They are considered as the external control. In the ideal case this is all we need to capture the essentials of thermodynamic machines, their possible cycles and efficiencies. This simple control model is then extended to include an internal time scale (phenomenological relaxation time) to allow for non-equilibrium effects. This will give us a direct access to finite time thermodynamics [9,19].

Such an approach is entirely within the spirit of thermodynamics, which itself can be formulated as a powerful control theory [2]. We assume that this system theoretical scheme captures the main features of any concrete implementation, for which coherence [8] does not play a major role. While there have been speculations about dramatic differences between classical and quantum machinery [20], (even claiming violations of the second law), we come here to the opposite conclusion: Classical and quantum mechanical machines behave essentially identical – to an extent, which is almost unbelievable. In fact, this

^a e-mail: jan.birjukow@daad-alumni.de

scale-invariance could hardly be expected, if one took it for granted that the pertinent (thermodynamic) concepts would, indeed, only apply in the thermodynamic limit of the system considered.

To be sure, we consider, in a sense, the ideal case. There are other important limitations in the nano-domain: as all length scales shrink, also the possibilities of thermal isolation become severely constrained (cf. [21]). This means, e.g., that the interaction with baths of different temperatures may no longer be assumed to be switched on and off at will. Leakage becomes unavoidable [11, 12, 17]. This aspect will presently be excluded, as are any implementation issues.

2 Model of Control

We consider a quantum system with discrete spectrum embedded in some environment. One can imagine three qualitatively different functions the environment could perform with respect to the system: a mechanical control, a decohering bath and a thermal bath considered as a statistical control.

Provided the weak coupling conditions are met, we assume that the mechanical control comes into action through a parameter-dependent spectrum of the effective Hamiltonian, $\{E_i^{\text{eff}}(\gamma)\}_{i=1}^N$, where N is the number of levels. One may regard this control as purely mechanical as long as the level occupations can survive the corresponding spectrum disturbance. It proves to be the case in the presence of decoherence rapid enough (time scale τ_{dec}) compared with $\dot{\gamma}$ [4].

This kind of decoherence can well originate from the appropriate part of the interaction between the system and its environment. In our model we assume such a decohering bath as a physical prerequisite of an adiabatic process. It has another important consequence, effectively making the coarse-grained density matrix ρ_t and the momentary hamiltonian $H^{\text{eff}}(\gamma_t)$ commute, excluding as well autonomous Schrödinger-dynamics. So we have to assume that our quantum system always stays in a mixed state determined by the diagonal elements of ρ in the respective energy representation, $\{p_i = \rho_{ii}\}_{i=1}^N$.

In order to introduce the statistical control, we postulate the existence of a one-parameter family of distributions, $\{\tilde{p}_i(\alpha)\}_{i=1}^N$, inherent to particular conditions of the contact between the system and its environment. These distributions are assumed to be stable in the sense that whenever the actual distribution p_i differs from $\tilde{p}_i(\alpha)$ at some given α , this deviation will decay on a time scale $\tau_R \gg \tau_{dec}$ according to

$$\dot{p}_i = -\tau_R^{-1}(p_i - \tilde{p}_i(\alpha)), \quad (1)$$

(relaxation time approximation). We shall refer to such $\tilde{p}_i(\alpha)$ as *attractor*.

Note that for τ_R small compared with the characteristic time of enforced α -parameter alterations, one gets

$$p_i = \tilde{p}_i(\alpha) \quad (2)$$

at all times, i.e. the so-called quasi-static limit [2].

In the very general case, all $E_i^{\text{eff}}(\gamma)$ had to be regarded as N independent functions that would make the model hardly tractable. In what follows we consider, instead, the special class of the spectral control

$$E_i^{\text{eff}}(\gamma) = g(\gamma) \cdot \epsilon_i, \quad (3)$$

where g is some monotonous function independent of i , and $\{\epsilon_i\}_{i=1}^N$ are to be regarded as a set of characteristic constants. Two pertinent examples resulting in $g(\gamma) = \gamma$ and $g(\gamma) = \gamma^{-2}$ are given in Sec 3.5.1 and Sec 3.5.2. This control allows to treat the distribution $\tilde{p}_i(\alpha)$ formally independent of γ even if the spectrum does explicitly enter the occupation numbers as, e.g., in the canonical case, cf. (15).

3 Quasi-static limit

The quasi-static limit plays a fundamental role in standard thermodynamics. Here it describes an important reference scenario: the limit of perfect control over a quantum system. Both the spectrum (3) and the energy distribution (2) are completely specified by γ and α taken to be external control parameters. Hence, as long as the thermodynamic quantities are properly defined, one can consider an arbitrary point in the (α, γ) -plane as a thermodynamic state implemented on the system under consideration.

3.1 Thermodynamic quantities

As follows from the foregoing, for the system's state, corresponding in the quasi-static limit to a certain point in the (α, γ) -plane, one can define the entropy S and the internal energy U [3] :

$$S(\alpha) := - \sum \ln \tilde{p}_i(\alpha) \cdot \tilde{p}_i(\alpha), \quad (4)$$

$$U(\alpha, \gamma) := g(\gamma) \sum \epsilon_i \cdot \tilde{p}_i(\alpha); \quad (5)$$

From (4) we observe, taking into account the normalization condition for $\{\tilde{p}_i(\alpha)\}_{i=1}^N$, that

$$\frac{dS}{d\alpha} = - \sum \ln \tilde{p}_i \left(\frac{d\tilde{p}_i}{d\alpha} \right). \quad (6)$$

In order to introduce the notion of temperature, we employ its formal definition [2, 3] as the conjugate variable to the entropy S :

$$T := \left(\frac{\partial U}{\partial S} \right)_{\gamma} = \left(\frac{\partial U}{\partial \alpha} \right)_{\gamma} \left(\frac{dS}{d\alpha} \right)^{-1}. \quad (7)$$

Together with (5) and (6) one gets

$$T(\alpha, \gamma) = g(\gamma)\Theta(\alpha)^{-1}, \quad (8)$$

where $\Theta(\alpha)$ stands for

$$\Theta(\alpha) := - \frac{\sum \ln \tilde{p}_i (d\tilde{p}_i/d\alpha)}{\sum \epsilon_i (d\tilde{p}_i/d\alpha)}, \quad (9)$$

a function depending solely on α .

Consider now the total differential of the internal energy (5) as a function of these control parameters [7]:

$$dU(\alpha, \gamma) = \left(\frac{\partial U}{\partial \alpha} \right)_{\gamma} d\alpha + \left(\frac{\partial U}{\partial \gamma} \right)_{\alpha} d\gamma. \quad (10)$$

Based on (7) we introduce the infinitesimal increment of heat, $\mathfrak{d}Q = TdS$:

$$\mathfrak{d}Q(\alpha, \gamma) := \left(\frac{\partial U}{\partial \alpha} \right)_{\gamma} d\alpha = g(\gamma) \sum \epsilon_i \left(\frac{d\tilde{p}_i}{d\alpha} \right) d\alpha. \quad (11)$$

As to the second term in (10), its meaning is the internal energy increment under constant α , in fact under constant entropy, cf. (4). It allows us to consider this term as work:

$$\mathfrak{d}W(\alpha, \gamma) := \left(\frac{\partial U}{\partial \gamma} \right)_{\alpha} d\gamma = \frac{dg}{d\gamma} \sum \epsilon_i \tilde{p}_i d\gamma. \quad (12)$$

Here, all the thermodynamic quantities have been defined based on a specific process in the control plane. Typical measurements (of temperature T , say) would rather exploit the dependence of a specific observable A , like the magnetization of a paramagnetic salt, on T .

3.2 Specific processes

So far as every point in the control plane (α, γ) represents some thermodynamic state, a continuous sequence of states, a process, can be defined by a path in this plane, eventually by some constraint on the accessible values of control parameter pairs, $f(\alpha, \gamma) = \text{const}$. For a concrete implementation the class of actually feasible processes will severely be restricted, just like for macroscopic machines.

Within our control theory framework the simplest examples for ideal conventional processes are *isentropes* and *isochores*, identified with $\alpha = \text{const}$ and $\gamma = \text{const}$, respectively. It is noteworthy that along an isentrope the temperature (8) is directly proportional to $g(\gamma)$. With $g(\gamma) = 1/\gamma$, for example, $T(\alpha, \gamma)$ will decrease with increasing γ :

$$T \propto \frac{1}{\gamma} \quad (13)$$

This is what happens to photons in a cavity of size $\gamma = L$, a phenomenon known also from the photon temperature reduction in our expanding universe (cosmic microwave background [22]). Another example is adiabatic demagnetization (magnetic cooling), with $\gamma = B$ and $g(\gamma) = \gamma$ (see Sec 3.5.1) resulting in $T \propto \gamma$.

Based on (8), the definition of an *isothermal* process is straight forward: $T(\alpha, \gamma) = \text{const}$ ($= T$). This constraint can be cast into the convenient form:

$$g(\gamma) = T \cdot \Theta(\alpha), \quad (14)$$

In which T plays the role of a scale factor: The shape of every isotherm is the same, depending eventually on the chosen form for $g(\gamma)$ and $\{\tilde{p}_i(\alpha)\}_{i=1}^N$, the attractor.

If, as a particular choice, one takes the *canonical attractor*:

$$\tilde{p}_i(\alpha) = Z_{\text{can}}^{-1} e^{-\alpha \epsilon_i}, \quad Z_{\text{can}} = \sum e^{-\alpha \epsilon_i}; \quad (15)$$

one finds from (9):

$$\Theta_{\text{can}}(\alpha) = \alpha. \quad (16)$$

With $g(\gamma) = \gamma$ the isotherms (14) will now be just straight lines in the control plane, $\gamma = \alpha T$ at constant T . With $g(\gamma) = \gamma^{-2}$ one would get $\gamma = 1/\sqrt{\alpha T}$, a sort of hyperbolae (see Fig. 1 and Fig. 2).

3.3 Heat and work

Bearing in mind the forthcoming analysis of various thermodynamic cycles, which underlie heat engine or heat pump operation, we consider the heat and work along specific processes. Integrating (11) and (12), one gets for the isotherms $g(\gamma) = T \cdot \Theta(\alpha)$:

$$Q_{\mathcal{T}} = T \sum \epsilon_i \int \Theta(\alpha) d\tilde{p}_i(\alpha); \quad (17a)$$

$$W_{\mathcal{T}} = T \sum \epsilon_i \int \tilde{p}_i(\alpha) \frac{d\Theta}{d\alpha} d\alpha; \quad (17b)$$

for the isentropes $\alpha = \text{const}$:

$$Q_S = 0; \quad (18a)$$

$$W_S = \Delta g(\gamma) \sum \epsilon_i \tilde{p}_i(\alpha); \quad (18b)$$

and for the isochores $\gamma = \text{const}$:

$$Q_{\gamma} = g(\gamma) \sum \epsilon_i \Delta \tilde{p}_i(\alpha); \quad (19a)$$

$$W_{\gamma} = 0; \quad (19b)$$

where Δ denotes the corresponding increment along the process line.

The sign of the heat flows $Q_{\mathcal{T}}$ and Q_{γ} is calculated in Appendix B for the case of the canonical $\tilde{p}_i(\alpha)$ (15). Such general sign statements cannot be proven for the work inputs $W_{\mathcal{T},S}$, as their sign depends, together with the rest, on the particular choice of $\{\epsilon_i\}_{i=1}^N$.

3.4 Carnot cycle

Provided the RHS of (9) behaves well, it is always possible to compose a closed path in the (α, γ) -plane from two isentropes and two isotherms – thus leading to a conventional Carnot cycle.

All the pertinent thermodynamic quantities, such as entropy (4), internal energy (5), temperature (8), heat (11) and work (12) are defined in the quasi-static limit in such a way that Eq. (10) turns into the Gibbsian fundamental form:

$$dU = TdS + \mathfrak{d}W, \quad (20)$$

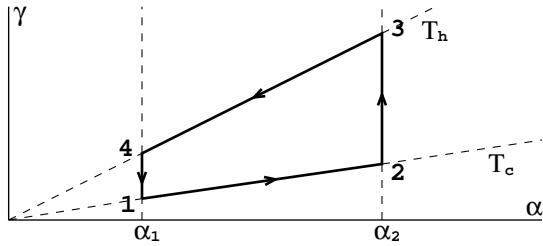


Fig. 1. Carnot's cycle in the (α, γ) -plane associated with the canonical attractor (15) and $g(\gamma) = \gamma$. It is composed by segments of isentropes $\alpha = \alpha_{1,2}$ and isotherms $\gamma = \alpha T_{c,h}$; ($T_h > T_c$). Arrows correspond to heat-engine performance.

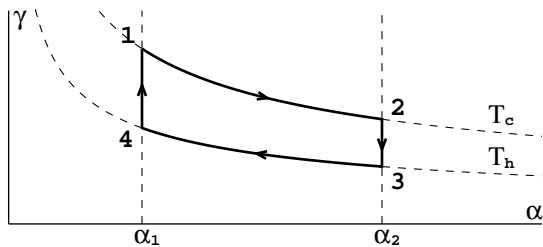


Fig. 2. As Fig. 1, but for $g(\gamma) = \gamma^{-2}$. The Carnot cycle is composed by segments of isentropes $\alpha = \alpha_{1,2}$ and isotherms $\gamma = 1/\sqrt{\alpha T_{c,h}}$; ($T_h > T_c$). Arrows correspond to heat-engine performance.

irrespective of $g(\gamma)$ or the chosen kind of attractor (2).

Thermodynamic efficiency of a heat engine cycle is defined as the ratio W_{out}/Q_{T_h} , where $W_{\text{out}} = -W_o > 0$ is the work output per cycle and $Q_{T_h} > 0$ is the heat input during the isothermal stage at the higher of two assigned temperatures: $T_h > T_c$. As usual, $Q_{T_c} < 0$ is supposed to be discarded, i.e. cannot be re-used. The validity of the Gibbsian fundamental form immediately leads to the Carnot efficiency [2]

$$\eta^c = 1 - \frac{T_c}{T_h}, \quad (21)$$

for any heat-engine cycle of Carnot's kind in the (α, γ) -plane independent of such model details as $\{\tilde{p}_i(\alpha)\}$ or $\{\epsilon_i\}$ or $g(\gamma)$.

Thus, the Carnot efficiency as a limiting fundamental value does not even require thermal states, only the control scheme with two parameters, as stated. The temperatures T_c, T_h would then only have a formal meaning, though. In some sense, this is a generalization of the well-known universality established in conventional macroscopic thermodynamics.

In order to present an illustrative example, we explore the case of the canonical attractor (15). The corresponding Carnot cycles are sketched in Fig. 1 and Fig. 2.

According to (80), for the heat-engine performance one must drive the cycle in Fig. 1 anticlockwise, while the cycle in Fig. 2 clockwise: These directions correspond to heat input for the high- and heat output for the low-temperature isothermal stage, respectively. Treating both cycles step-

wise based on (17) and (18), one explicitly gets the Carnot efficiency (21), as expected.

Two examples for other possible choices of the attractor type are given in Appendix A. These examples illustrate the diversity of forms the Carnot cycles can have in the control space (α, γ) depending on the underlying attractor. In the quasi-static limit, however, all of them share the standard rectangular form in the (S, T) -space (Fig. 4). Also the efficiency is always given by the Carnot value; in this sense, one cannot win anything by trying to implement exotic distribution functions.

3.5 Otto cycle

It is well-known that the universality established for the Carnot cycle does not carry over to other cycle types. This means that the resulting efficiencies $\eta \leq \eta^c$ would then depend on the actual control functions $g(\gamma)$ and $\tilde{p}_i(\alpha)$.

The Otto cycle is in some sense the most fundamental quantum thermodynamic cycle: On the isentropes, there is only a change of the spectrum while on the isochors only the occupation numbers are changing. Most of the theoretically discussed quantum thermodynamic machines perform, in effect, the Otto cycle [8, 15, 23].

Fig. 3 shows the Otto cycle in the (α, γ) -plane. As the Carnot cycle discussed above, this cycle must be driven anticlockwise or clockwise, depending on the choice of $g(\gamma)$, in order to get the heat-engine performance.

If the function $g(\gamma)$ is increasing, (18) and (19) lead to the efficiency:

$$\eta^O = 1 - \frac{g(\gamma_1)}{g(\gamma_2)}. \quad (22)$$

For a 2-level system, one gets, identifying

$$\Delta(\gamma) = g(\gamma)(\epsilon_2 - \epsilon_1) \quad (23)$$

the well-known result [24]

$$\eta = 1 - \frac{\Delta(\gamma_1)}{\Delta(\gamma_2)}, \quad (24)$$

which is often mistaken as representing the Carnot efficiency [25].

With decreasing $g(\gamma)$ one must drive the cycle clockwise to get a heat-engine. The efficiency is then given by

$$\eta'^O = 1 - \frac{g(\gamma_2)}{g(\gamma_1)}, \quad (25)$$

In any case, the efficiency only depends on the relative compression, just like for the classical Otto cycle [1].

To compare these results with the efficiency of the Carnot cycle, we consider the canonical case (14–16) to get

$$\eta^O = 1 - \frac{T_c \alpha_2}{T_h \alpha_1} \quad (26a)$$

$$\eta'^O = 1 - \frac{T'_c \alpha_2}{T'_h \alpha_1} \quad (26b)$$

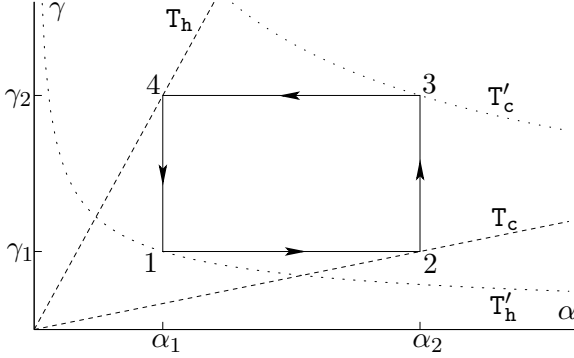


Fig. 3. Otto cycle in the (α, γ) -plane. The isentropes are given by $\alpha = \text{const}$ and the isochors by $\gamma = \text{const}$. The dashed lines are canonical isotherms with the highest and lowest temperature of the cycle for $g(\gamma) = \gamma$, while the dotted ones hold for $g(\gamma) = \gamma^{-2}$.

where T_c (T'_c) is the lowest temperature and T_h (T'_h) the highest temperature along the cycle. As shown in Fig. 3, T_c is reached at point 2 and T_h at point 4 for increasing $g(\gamma)$, whereas for decreasing $g(\gamma)$ T'_c is reached at point 3 and T'_h at point 1 (cf. [8]). As one can see, the efficiency of the Otto cycle remains below the Carnot value. Formally, the Carnot efficiency is reached for $\alpha_2 = \alpha_1$, when the total work output of the machine vanishes (cf. [15]).

In the following we shall give two examples of spectral control:

3.5.1 Example: Spin in a magnetic field

For a spin in the magnetic field B , $E_i \propto B$ holds. Identifying the control parameter γ with B , we have

$$g(\gamma) = \gamma \quad (27)$$

and therefore the efficiency (22) simply reads

$$\eta_{\text{spin}}^{\circ} = 1 - \frac{\gamma_1}{\gamma_2}, \quad (28)$$

3.5.2 Example: Particle in a box

Consider a particle in a box of length L [20]. The energy levels depend on the length as $E_i \propto 1/L^2$. This length can thus be used to control the spectrum. Identifying γ with L , we have:

$$g(\gamma) = \frac{1}{\gamma^2} \quad (29)$$

Because $g(\gamma)$ is decreasing here, we have to take (25) as the efficiency:

$$\eta_{\text{box}}^{\circ} = 1 - \left(\frac{\gamma_1}{\gamma_2} \right)^2 \quad (30)$$

4 Driven non-equilibrium

Now we are going to re-define the thermodynamic quantities introduced in Sec. 3, allowing for deviations of the momentary distribution $\{p_i\}$ from the attractor $\{\tilde{p}_i(\alpha)\}$. In this way we extend the scope of our consideration beyond the quasi-static limit (2) including processes with the cycle times comparable with the relaxation time τ_R introduced in (1).

4.1 Beyond the quasi-static limit

According to (1), the probabilities p_i no longer depend just on the momentary control $\alpha(t)$ as in the quasi-static limit; they also become dependent on their past history. Nevertheless, they are quite well computable, as soon as $\alpha(t)$ and the initial values are defined, and one can still define the entropy and the internal energy just by replacing $\tilde{p}_i(\alpha)$ in (4) and (5) with p_i .

We define the non-equilibrium work $\text{d}W^*$ as the increment of the internal energy due to variations of the mechanical control γ :

$$\text{d}W^* = \left(\frac{\partial U^*}{\partial \gamma} \right)_{p_i} d\gamma = \frac{d\gamma}{d\gamma} \sum \epsilon_i p_i d\gamma; \quad (31)$$

while the non-equilibrium heat $\text{d}Q^*$ based on the first law:

$$\text{d}Q^* = dU^* - \text{d}W^* = g(\gamma) \sum \epsilon_i dp_i. \quad (32)$$

(By an asterisk we indicate the renormalization due to non-equilibrium.)

The renormalized temperature T^* will be taken to remain a control variable asking for the response of U^* to a change of the statistical control α . Note that the non-equilibrium distribution $\{p_i\}$ can formally be represented as

$$p_i(\alpha, \Delta p_i) = \tilde{p}_i(\alpha) + \Delta p_i, \quad (33)$$

with deviations Δp_i due to the dynamical response of the system. Being well computable by means of the relaxation equations (1), they are, however, not under our direct control. That is why we seek the response to a change of α at some given $\{\Delta p_i\}$:

$$T^* = \left(\frac{\partial U^*}{\partial \alpha} \right)_{\gamma, \Delta p_i} \left(\frac{\partial S^*}{\partial \alpha} \right)_{\Delta p_i}^{-1}. \quad (34)$$

Such a definition results in (cf. (8)):

$$T^* = -g(\gamma) \frac{\sum \epsilon_i (d\tilde{p}_i/d\alpha)}{\sum \ln p_i (d\tilde{p}_i/d\alpha)}. \quad (35)$$

The quantity T^* , determined in this way, we shall call *renormalized process temperature*.

In the following we assume the time-dependence of the control parameter $\alpha(t)$ to be:

$$\alpha = \alpha_0 + vt, \quad (36)$$

where v may be positive or negative. Of course, there are other possible choices, indicating that more details of the control may become important.

With the attractor $\{\tilde{p}_i(\alpha)\}$ driven according to (36), the relaxation equations (1) take the form:

$$(dp_i/d\alpha) = -(v\tau_R)^{-1}(p_i - \tilde{p}_i(\alpha)) \quad (37)$$

and yield the solutions:

$$p_i = p_i^{(0)} e^{-\frac{\alpha - \alpha_0}{v\tau_R}} + (v\tau_R)^{-1} \int_{\alpha_0}^{\alpha} \tilde{p}_i(\alpha') e^{-\frac{\alpha - \alpha'}{v\tau_R}} d\alpha'. \quad (38)$$

This means that, in a sense, the p_i could still be considered as an explicit function of α as soon as their initial values p_i^0 and α_0 are specified by the given process history.

4.2 Renormalized process temperature

In order to understand what happens with the process temperature along non-isentropic paths in the control plane, we consider the asymptote under very slow driving, $(v\tau_R/\Delta\alpha) \ll 1$, when the following expansion holds (see App. C):

$$p_i = \tilde{p}_i(\alpha) - v\tau_R \frac{d\tilde{p}_i}{d\alpha} + o\left[\frac{v\tau_R}{\Delta\alpha}\right], \quad (39)$$

where $\Delta\alpha$ denotes the increment of α in the course of the process. Inserting this expansion into (35) and keeping terms up to first order in $(v\tau_R/\Delta\alpha)$, one gets:

$$T^* = T(\alpha, \gamma) \left(1 + v\tau_R \frac{\sum (1/\tilde{p}_i)(d\tilde{p}_i/d\alpha)^2}{\sum \ln \tilde{p}_i(d\tilde{p}_i/d\alpha)} \right) + o\left[\frac{v\tau_R}{\Delta\alpha}\right], \quad (40)$$

observing as well the definition (8) for the temperature $T(\alpha, \gamma)$ in the quasi-static limit.

Of course, any chosen process line $f(\alpha, \gamma) = \text{const}$ implies a certain relationship between γ and α . In the canonical case (15) and when the process is taken to run along the line $g(\gamma) = T \cdot \alpha$, which would be an isotherm in the quasi-static limit, cf. (14), Eq. (40) reduces to:

$$T^*(\alpha) = T \left(1 + \frac{v\tau_R}{\alpha} \right) + o\left[\frac{v\tau_R}{\Delta\alpha}\right], \quad (41)$$

For a Carnot machine cycle (Fig. 1 and Fig. 2) this means, compared with the quasi-static limit, that the dynamically renormalized process temperature is increased for increasing α ($v > 0$, contact with a heat sink) and decreased for decreasing α ($v < 0$, heat source). Temperature shifts like those following from (41) have *ad hoc* been introduced in Curzon and Ahlborn's finite time analysis of the heat engine efficiency [19]. Already at $v\tau_R \approx 1$, however, the ST loop proper is dominated by counteracting non-equilibrium excursions (Fig. 4, cf. [9]), which indicates that there will be no machine function left at high driving speed (cf. Sec 5.1).

One may wonder, if such a behaviour of the temperature as shown in Fig. 4 really can be observed in physical systems. Indeed this seems to be the case: Very recently such a temperature pattern was found in numerical experiments for the finite-time Carnot cycle of a classical ideal gas by means of molecular dynamics simulations [27].

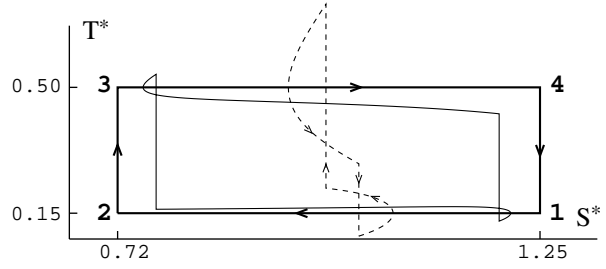


Fig. 4. Carnot cycle in the (S^*, T^*) -plane. Both cycles from Fig. 1 and Fig. 2 look similar here. The rectangle denotes the perfect Carnot cycle in the quasi-static limit $v\tau_R = 0$. The solid line corresponds to a stationary cyclic regime at $v\tau_R = 0.09$; the dashed one – at $v\tau_R = 0.9$. This is a result of numerical simulations in accordance with $S^* := -\sum \ln p_i \cdot p_i$ and (35), with p_i under relaxation (38). The set of constants $\{\epsilon_i\}_{i=1}^N$ is chosen here to be $\{-3/2; -1/2; 1/2; 3/2\}$.

4.3 Renormalized heat and work

Consider the renormalized heat and work along those specific processes underlying Carnot and Otto cycles. One has to integrate now (32) and (31) along the corresponding lines in the (α, γ) -plane. In the case of the canonical isotherm $g(\gamma) = \alpha T$ this leads to the integrals $\int_{\alpha_0}^{\alpha} \alpha' dp_i$ and $\int_{\alpha_0}^{\alpha} p_i d\alpha'$, with the probabilities p_i under relaxation as given by (38). The latter is readily achievable directly from the relaxation equation (37):

$$\int_{\alpha_0}^{\alpha} p_i d\alpha' = \int_{\alpha_0}^{\alpha} \tilde{p}_i(\alpha') d\alpha' - v\tau_R (p_i - p_i^{(0)}), \quad (42)$$

immediately followed by:

$$\begin{aligned} \int_{\alpha_0}^{\alpha} \alpha' dp_i &= \int_{\alpha_0}^{\alpha} \alpha' d\tilde{p}_i(\alpha') + \alpha (p_i - \tilde{p}_i(\alpha)) \\ &\quad - \alpha_0 (p_i^{(0)} - \tilde{p}_i(\alpha_0)) + v\tau_R (p_i - p_i^{(0)}). \end{aligned} \quad (43)$$

Renormalized isothermal heat and work are thus in the canonical case:

$$\begin{aligned} Q_{\mathcal{T}}^* &= Q_{\mathcal{T}} + q + q' + q'', \\ q &:= v\tau_R T \sum \epsilon_i (p_i - p_i^{(0)}), \\ q' &:= -\alpha_0 T \sum \epsilon_i (p_i^{(0)} - \tilde{p}_i(\alpha_0)), \\ q'' &:= \alpha T \sum \epsilon_i (p_i - \tilde{p}_i(\alpha)); \end{aligned} \quad (44a)$$

$$\begin{aligned} W_{\mathcal{T}}^* &= W_{\mathcal{T}} + w, \\ w &:= -v\tau_R T \sum \epsilon_i (p_i - p_i^{(0)}) = -q; \end{aligned} \quad (44b)$$

Again, the respective renormalized quantities are denoted by an asterisk, while the heat and work in the quasi-static limit (right hand side) are defined according to (17) with $\Theta(\alpha) = \alpha$.

Integration along the isentropic line $\alpha = \text{const}$ yields zero for the heat and $\Delta g \sum \epsilon_i p_i^{(0)}$ for the work, due to

the conservation (ideal in our model) of the respective distribution — the results are similar to those obtained in the quasi-static limit (18):

$$Q_S^* = 0; \quad (45a)$$

$$W_S^* = W_S + w',$$

$$w' := \Delta g(\gamma) \sum \epsilon_i \left(p_i^{(0)} - \tilde{p}_i(\alpha_0) \right); \quad (45b)$$

Finally, for the isochores $\gamma = \text{const}$ one gets:

$$Q_\gamma^* = Q_\gamma + \tilde{q} + \tilde{\tilde{q}},$$

$$\tilde{q} := -g(\gamma) \sum \epsilon_i \left(p_i^{(0)} - \tilde{p}_i(\alpha_0) \right),$$

$$\tilde{\tilde{q}} := g(\gamma) \sum \epsilon_i \left(p_i - \tilde{p}_i(\alpha) \right); \quad (46a)$$

$$W_\gamma^* = 0; \quad (46b)$$

where Q_γ^* , as well as W_S^* before, is formally expressed through its quasi-static value.

5 Finite-time thermodynamic cycles

In order to realize a cyclic process in the (α, γ) -control plane, we have to assign $\alpha(t)$ for both running directions between the turning points α_1 and α_2 . We allow for different driving speeds, namely:

$$\alpha_{1 \rightarrow 2}(t) = \alpha_1 + \kappa t; \quad \alpha_{2 \rightarrow 1}(t) = \alpha_2 - \lambda \kappa t, \quad (47)$$

with $\kappa, \lambda > 0$.

Taking (38) with $v = \kappa$ and $v = -\lambda\kappa$, respectively, one comes up with the following distributions at the turning points in the stationary cyclic regime:

$$p_i^{(1)} = \left(e^{\frac{\Delta\alpha}{\lambda\kappa\tau_R}} - e^{-\frac{\Delta\alpha}{\kappa\tau_R}} \right)^{-1} \cdot (\kappa\tau_R)^{-1} \quad (48a)$$

$$\times \int_{\alpha_1}^{\alpha_2} \tilde{p}_i(\alpha') \left(e^{-\frac{\alpha_2 - \alpha'}{\kappa\tau_R}} + \frac{1}{\lambda} e^{\frac{\alpha_2 - \alpha'}{\lambda\kappa\tau_R}} \right) d\alpha';$$

$$p_i^{(2)} = \left(e^{\frac{\Delta\alpha}{\kappa\tau_R}} - e^{-\frac{\Delta\alpha}{\lambda\kappa\tau_R}} \right)^{-1} \cdot (\kappa\tau_R)^{-1} \quad (48b)$$

$$\times \int_{\alpha_1}^{\alpha_2} \tilde{p}_i(\alpha') \left(e^{\frac{\alpha' - \alpha_1}{\kappa\tau_R}} + \frac{1}{\lambda} e^{-\frac{\alpha' - \alpha_1}{\lambda\kappa\tau_R}} \right) d\alpha';$$

5.1 Finite-time Carnot cycle

Consider now the Carnot cycle (Fig. 1 and Fig. 2) driven with the speed $v = \kappa$ on the low- and $v = -\lambda\kappa$ on the high-temperature isothermal stage according to (47). The established cyclic regime implies here the distribution (48a) at the points “1” and “4” and (48b) at the points “2” and “3” of the cycle — there is no relaxation on the isentropes, as discussed before.

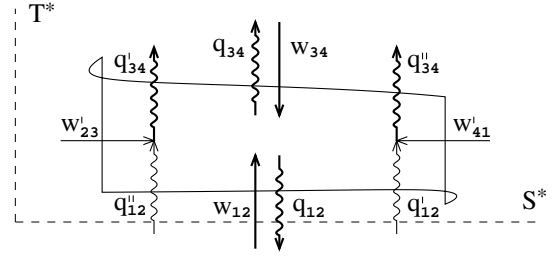


Fig. 5. Corrections (49) and (50) to the quasi-static heat and work along the stages of Carnot-like machine cycle (Fig. 4). Straight lines denote work, wavy ones – heat. Arrows pointing into the contour indicate energy flows into the system. (The primary, quasi-static contributions (17) and (18) providing the machine action are not shown.)

With (44) we get the following correction terms to the quasi-static heat and work along the isotherms $1 \rightarrow 2$ and $3 \rightarrow 4$, respectively:

$$q_{12} = \kappa\tau_R T_c \sum \epsilon_i \left(p_i^{(2)} - p_i^{(1)} \right) < 0;$$

$$q'_{12} = -\alpha_1 T_c \sum \epsilon_i \left(p_i^{(1)} - \tilde{p}_i(\alpha_1) \right) > 0;$$

$$q''_{12} = \alpha_2 T_c \sum \epsilon_i \left(p_i^{(2)} - \tilde{p}_i(\alpha_2) \right) > 0;$$

$$q_{34} = \lambda(T_h/T_c) q_{12} < 0;$$

$$q'_{34} = -(T_h/T_c) q''_{12} < 0;$$

$$q''_{34} = -(T_h/T_c) q'_{12} < 0;$$

$$w_{12} = -q_{12} > 0;$$

$$w_{34} = -q_{34} > 0. \quad (49)$$

Eq. (45b) yields the correction to the quasi-static work along the isentropes $2 \rightarrow 3$ and $4 \rightarrow 1$, respectively:

$$w'_{23} = \alpha_2 \Delta T \sum \epsilon_i \left(p_i^{(2)} - \tilde{p}_i(\alpha_2) \right) > 0;$$

$$w'_{41} = -\alpha_1 \Delta T \sum \epsilon_i \left(p_i^{(1)} - \tilde{p}_i(\alpha_1) \right) > 0; \quad (50)$$

Here we have observed $\Delta g(\gamma) = \alpha \Delta T$, which follows from (14) and (16).

The inequalities (sign) in (49) and (50) are proven in Appendix B. The sign of every correction term remains the same for any κ and λ , allowing us to sketch their general scheme in Fig. 5. Of course, all the terms listed here relate to the corresponding cycle step as a whole, not allowing for physical separation. Nevertheless, such a representation proves to be useful for the purpose of the heat and work transfer analysis in various driving speed regimes as well as in comparison with the cycles of other kinds.

In the limit of very slow driving, $(\kappa\tau_R/\Delta\alpha) \ll 1$, one has (see App. C):

$$p_i^{(2)} - p_i^{(1)} = \tilde{p}_i(\alpha_2) - \tilde{p}_i(\alpha_1) + \mathcal{O}[\kappa\tau_R],$$

$$p_i^{(1)} - \tilde{p}_i(\alpha_1) = \lambda\kappa\tau_R \left(\frac{d\tilde{p}_i}{d\alpha} \right)_{\alpha_1} + o[\kappa\tau_R],$$

$$p_i^{(2)} - \tilde{p}_i(\alpha_2) = -\kappa\tau_R \left(\frac{d\tilde{p}_i}{d\alpha} \right)_{\alpha_2} + o[\kappa\tau_R]; \quad (51)$$

which means that all the terms in (49) and (50) are of first order in $\kappa\tau_R$. In Sec. 5.2 these results will be used in order to reveal the fast degradation of the machine efficiency with increasing driving speed κ .

In the limit of very fast driving, $(\Delta\alpha/\kappa\tau_R) \ll 1$, the terms above can be shown to be (App. C):

$$p_i^{(2)} - p_i^{(1)} = -\frac{\Delta\alpha}{\lambda(\kappa\tau_R)^2} \cdot \mathcal{I}_i + o\left[\left(\frac{\Delta\alpha}{\kappa\tau_R}\right)^2\right], \quad (52)$$

$$p_i^{(1;2)} - \tilde{p}_i(\alpha_{1;2}) = \bar{p}_i - \tilde{p}_i(\alpha_{1;2}) + \frac{1-\lambda}{\lambda\kappa\tau_R} \cdot \mathcal{I}_i + o\left[\frac{\Delta\alpha}{\kappa\tau_R}\right];$$

where

$$\begin{aligned} \mathcal{I}_i &:= \frac{1}{\Delta\alpha} \int_{\alpha_1}^{\alpha_2} (\bar{p}_i - \tilde{p}_i(\alpha)) \alpha \, d\alpha, \\ \bar{p}_i &:= \frac{1}{\Delta\alpha} \int_{\alpha_1}^{\alpha_2} \tilde{p}_i(\alpha) d\alpha; \end{aligned} \quad (53)$$

– the latter being the average of $\tilde{p}_i(\alpha)$ over the interval $[\alpha_1; \alpha_2]$.

The result (52) supports the intuitive expectation for the collapse of the cycle on (S^*, T^*) -space (Fig. 4) at high driving speed κ . The only energy flows surviving $\kappa\tau_R \rightarrow \infty$ are the total work along the isentropic stages, $W_{23;41}^*$, and the quasi-static part of the work along the isotherms:

$$\begin{aligned} W_{23;41}^* &= \pm \Delta T \alpha_{2;1} \sum \epsilon_i \bar{p}_i; \\ W_{12;34} &= \pm T_{c;h} \Delta\alpha \sum \epsilon_i \bar{p}_i. \end{aligned} \quad (54)$$

The heat flows Q^* in the limit $(\Delta\alpha/\kappa\tau_R) \ll 1$ are:

$$\begin{aligned} Q_{12}^* &= -T_c \frac{\Delta\alpha}{\kappa\tau_R} \sum \epsilon_i \mathcal{I}_i + o\left[\frac{\Delta\alpha}{\kappa\tau_R}\right]; \\ Q_{34}^* &= -T_h \frac{\Delta\alpha}{\lambda\kappa\tau_R} \sum \epsilon_i \mathcal{I}_i + o\left[\frac{\Delta\alpha}{\kappa\tau_R}\right], \end{aligned} \quad (55)$$

negative on the both isothermal stages (App. B). Sure, there is no machine action left at $\kappa\tau_R \gg 1$.

A comment must be made concerning the scheme in Fig. 5. The triples $(\mathfrak{q}'_{12}; \mathfrak{w}'_{41}; \mathfrak{q}''_{34})$ and $(\mathfrak{q}''_{12}; \mathfrak{w}'_{23}; \mathfrak{q}'_{34})$ look like effective heat-pumps, counteracting the primary machine action along the cycle. This impression is supported by the balance relations, following from (49) and (50):

$$\begin{aligned} \mathfrak{q}'_{12} + \mathfrak{w}'_{41} + \mathfrak{q}''_{34} &= 0; \\ \mathfrak{q}''_{12} + \mathfrak{w}'_{23} + \mathfrak{q}'_{34} &= 0, \end{aligned} \quad (56)$$

and may insinuate the idea of a crossover to a heat pump at some values of κ and λ . As a matter of fact, this never happens for a cycle of the kind under consideration; it is proven in App. D that $Q_{12}^* < 0$ always holds — there is no heat absorption from the cold bath as a result of the low-temperature isothermal step of the cycle.

We conclude this paragraph with graphs (Fig. 6 and Fig. 7), which illustrate the degradation of the Carnot cycle's machine action with the growing driving velocity.

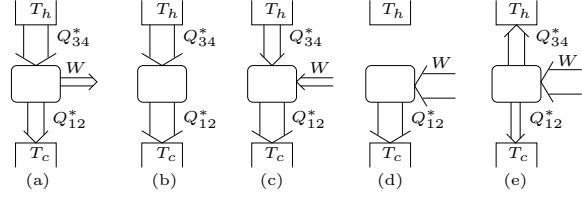


Fig. 6. The development of the Carnot cycle can be divided into five steps: For small $\kappa\tau_R$, the cycle works as a heat engine (a). At a certain velocity, the total work vanishes, and there is only heat flowing from the hot to the cold bath (b). After that point, work has changed its sign (c). Then there exists a velocity, where Q_{34}^* vanishes. The work therefore is completely transformed into heat, flowing into the cold bath (d). Finally, heat is flowing in the cold as well as in the hot bath (e), which corresponds to the high driving speed limit, discussed before. Note that the size of the arrows is rescaled at each picture: All components of heat and work tend to decrease for increasing velocity as shown in Fig. 7.

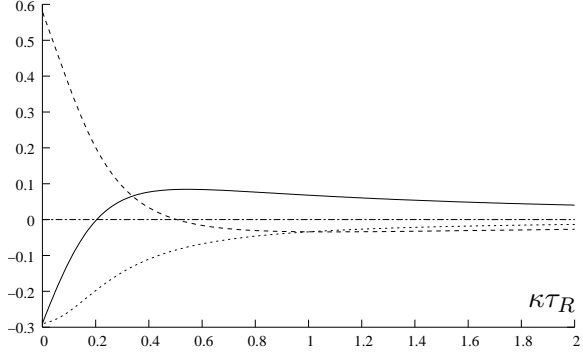


Fig. 7. Behaviour of W_0^* (solid lines), Q_{34}^* (dashed lines) and Q_{12}^* (dotted lines) with increasing velocity, typical for a Carnot cycle. The chosen parameters are $\{\epsilon_i\}_{i=1}^N = \{-3/2; -1/2; 1/2; 3/2\}$ and $\alpha_1 = 0.2$, $\alpha_2 = 0.8$, $T_c = 1$, $T_h = 2$. As one can see, both W_0^* and Q_{34}^* change their sign at certain finite velocities yet, while Q_{12}^* always stays negative.

5.2 The efficiency at maximum power output

In the following we restrict ourselves to corrections to the quasi-static heat and work along the cycle stages linear in the driving speed. In the appropriate limit (51) eqs. (49–50) result in

$$\begin{aligned} \{\mathfrak{w}_{12}; \mathfrak{w}_{34}\} &= \{-\mathfrak{q}_{12}; -\mathfrak{q}_{34}\} = \{T_c; \lambda T_h\} \times \kappa\tau_R a, \\ \text{where } a &:= \sum \epsilon_i (\tilde{p}_i(\alpha_1) - \tilde{p}_i(\alpha_2)) > 0; \end{aligned} \quad (57a)$$

$$\begin{aligned} \{\mathfrak{q}'_{12}; \mathfrak{w}'_{41}; \mathfrak{q}''_{34}\} &= \{T_c; \Delta T; -T_h\} \times \lambda\kappa\tau_R b', \\ \text{where } b' &:= \alpha_1 \sum \epsilon_i (-d\tilde{p}_i/d\alpha)_{\alpha_1} > 0; \end{aligned} \quad (57b)$$

$$\begin{aligned} \{\mathfrak{q}''_{12}; \mathfrak{w}'_{23}; \mathfrak{q}'_{34}\} &= \{T_c; \Delta T; -T_h\} \times \kappa\tau_R b'', \\ \text{where } b'' &:= \alpha_2 \sum \epsilon_i (-d\tilde{p}_i/d\alpha)_{\alpha_2} > 0. \end{aligned} \quad (57c)$$

(The inequalities are proven in Appendix B.)

We assume, in addition, that the relative part of the time per cycle spent on isothermal steps remains always the same, say δ . Hence, the period Δt for one full cycle turns out to be [19]:

$$\Delta t = \frac{\Delta\alpha}{\delta\kappa} \frac{\lambda + 1}{\lambda}. \quad (58)$$

The ratio of the total work output per full cycle, $W_{\text{out}}^* = -W_{\text{o}}^* > 0$, to the heat absorbed on the high-temperature isothermal step, $Q_{\mathcal{T}_h}^*$, yields the efficiency η^* . As follows from the scheme on Fig. 5 and (57), one gets:

$$\eta^* = \frac{W_{\text{out}} - \kappa\tau_R((T_c + \lambda T_h)a + \lambda\Delta T b' + \Delta T b'')}{Q_{\mathcal{T}_h} - \kappa\tau_R T_h(\lambda(a + b') + b'')} \quad (59)$$

One easily convinces oneself that this result is bounded from above by the quasi-static Carnot limit

$$\frac{W_{\text{out}}}{Q_{\mathcal{T}_h}} = \eta^C = \frac{\Delta T}{T_h}, \quad (60)$$

reached at $\kappa = 0$. The power output $\mathcal{P}^* = W_{\text{out}}^*/\Delta t$ is given by

$$\mathcal{P}^* = \frac{\delta\kappa\lambda}{\Delta\alpha(\lambda + 1)} \times \left(W_{\text{out}} - \kappa\tau_R((T_c + \lambda T_h)a + \lambda\Delta T b' + \Delta T b'') \right) \quad (61)$$

which confirms that $\mathcal{P}^* = 0$ for $\kappa = 0$, i.e. for the maximum Carnot efficiency η^C .

Our aim now is to maximize \mathcal{P}^* with respect to parameters κ and λ and to find the corresponding thermodynamic efficiency (59).

The condition for an extremum, $\partial_\kappa \mathcal{P}^* = \partial_\lambda \mathcal{P}^* = 0$, yields

$$\begin{cases} W_{\text{out}} = 2\kappa\tau_R((T_c + \lambda T_h)a + \lambda\Delta T b' + \Delta T b''), \\ W_{\text{out}} = \kappa\tau_R((T_c + \lambda T_h)a + \lambda\Delta T b' + \Delta T b'') \\ \quad + \kappa\tau_R\lambda(\lambda + 1)(T_h a + \Delta T b'). \end{cases} \quad (62)$$

It follows from (62) that the maximum of \mathcal{P}^* occurs at:

$$\lambda^2 = \frac{T_c}{T_h} \cdot \frac{1 + \Delta T b''/T_c a}{1 + \Delta T b'/T_h a}. \quad (63)$$

Eliminating now $Q_{\mathcal{T}_h}$, W_{out} and λ in (59) by means of (60) and those maximum conditions, one obtains:

$$\eta_{\text{max}\mathcal{P}}^* = \eta^C \left(1 + \frac{1}{\sqrt{(1 + \frac{\Delta T b'}{T_h a})(1 + \frac{\Delta T b''}{T_c a})}} \sqrt{\frac{T_c}{T_h}} \right)^{-1}. \quad (64)$$

As one can see, while the formal upper bound for $\eta_{\text{max}\mathcal{P}}^*$ is still Carnot's η^C , the lower bound is the celebrated Curzon-Ahlborn efficiency [19,26]:

$$\eta^{CA} = 1 - \sqrt{\frac{T_c}{T_h}}, \quad (65)$$

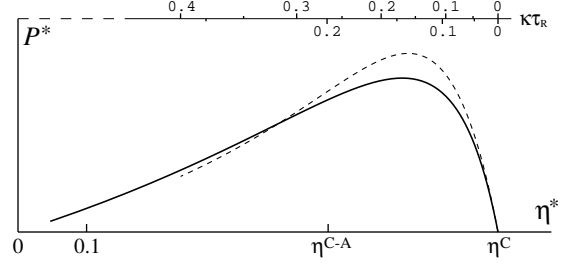


Fig. 8. Power output $\mathcal{P}^* = W_{\text{out}}^*/\Delta t$ (arbitrary units) vs. Efficiency $\eta^* = W_{\text{out}}^*/Q_{\mathcal{T}_h}^*$. The solid line and the lower $\kappa\tau_R$ -scale correspond to the linear driving speed approximation (59) and (61), at $\lambda = 0.756$ (63). The dashed line and the upper $\kappa\tau_R$ -scale correspond to exact calculations based on (48), when the maximal power output appears to be achieved at $\lambda = 1.040$.

attainable in the case, when $\Delta T b'/T_h a$ and $\Delta T b''/T_c a$ can be neglected.

Formally, it is the triples $(q'_{12}; w'_{41}; q''_{34})$ and $(q''_{12}; w'_{23}; q'_{34})$ in the finite-time corrections to the heat and work (57), that makes $\eta_{\text{max}\mathcal{P}}^* > \eta^{CA}$. In fact, they originate from the discrepancy between the steered attractor $\{\tilde{p}_i(\alpha)\}$ and the values of p_i (48) lagging behind at the cycle turning points. It is clear, that such a *residual non-equilibrium effect* could not emerge in the purely phenomenological thermodynamic setup by Curzon and Ahlborn [19]. Nevertheless, it has been observed for the classical ideal gas in recent numerical experiments [27].

To be sure, the higher efficiency $\eta_{\text{max}\mathcal{P}}^*$ does not mean any practical gain in the machine action here, because the corrections mentioned above do reduce both the heat $Q_{\mathcal{T}_h}$ absorbed from the high-temperature bath and the work output W_{out}^* per cycle, cf. (59).

Applying Taylor's formula for $\tilde{p}_i(\alpha)$ in (57) provides a rough estimate for the terms $\Delta T b'/T_h a$ and $\Delta T b''/T_c a$. Observing (16) and (14) as well, one gets:

$$\frac{\Delta T b'}{T_h a} \approx \frac{(\Delta g)_{S_1}}{(\Delta g)_{\mathcal{T}_h}}; \quad \frac{\Delta T b''}{T_c a} \approx \frac{(\Delta g)_{S_2}}{(\Delta g)_{\mathcal{T}_c}}, \quad (66)$$

where $(\Delta g)_{\mathcal{T}_{c,h}}$ and $(\Delta g)_{S_{1,2}}$ stand for increments of function $g(\gamma)$ along the corresponding isotherms and isentropes.

Thus, one can expect Curzon-Ahlborn's result (65) for Carnot cycles with small enough ΔT and large enough $\Delta\alpha$ (eventually large enough ΔS). With the cycle parameters we have taken for our illustrations (Fig. 1 and Fig. 2) it is obviously not the case, however, and the optimum η , indeed, lies between the Carnot and the Curzon-Ahlborn bounds, both for the exact and the linearized calculation (Fig. 8).

5.3 Finite-time Otto cycle

We finally turn to the Otto machine cycle shown in Fig. 3, driven now with finite speed. Again we allow for two different speeds on the isochors, in accordance with (47), and no bath coupling and no relaxation are assumed along the isentropes. The distributions p_i at the cycle's turning

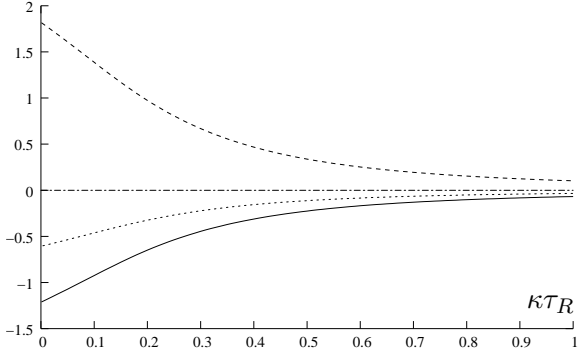


Fig. 9. Behaviour of W_0^* (solid lines), Q_{34}^* (dashed lines) and Q_{12}^* (dotted lines) with increasing velocity for an Otto cycle of a four level system. The chosen parameters are $\{\epsilon_i\}_{i=1}^N = \{-3/2; -1/2; 1/2; 3/2\}$ and $\alpha_1 = 0.2, \alpha_2 = 0.8, \gamma_1 = 1, \gamma_2 = 3$. As one can see, the ratio $-W_0^*/Q_{34}^*$, which defines the efficiency, always stays the same.

points “1” (“4”) and “2” (“3”) are again given by (48a) and (48b), respectively.

The heat and work along the cycle steps then follow from (45) and (46):

$$\begin{aligned} Q_{12}^* &= g(\gamma_1) \sum \epsilon_i (p_i^{(2)} - p_i^{(1)}) < 0, \\ W_{23}^* &= [g(\gamma_2) - g(\gamma_1)] \sum \epsilon_i p_i^{(2)}, \\ Q_{34}^* &= -g(\gamma_2) \sum \epsilon_i (p_i^{(2)} - p_i^{(1)}) > 0, \\ W_{41}^* &= -[g(\gamma_2) - g(\gamma_1)] \sum \epsilon_i p_i^{(1)}; \end{aligned} \quad (67)$$

the inequalities are proven in App. B.

The efficiency can now easily be calculated: With increasing $g(\gamma)$ we get

$$\eta^{*O} = \frac{-(W_{23}^* + W_{41}^*)}{Q_{34}^*} = 1 - \frac{g(\gamma_1)}{g(\gamma_2)} \quad (68)$$

With decreasing $g(\gamma)$, one has to run the cycle clockwise to achieve heat-engine performance, which results in the efficiency

$$\eta^{*O} = 1 - \frac{g(\gamma_2)}{g(\gamma_1)}, \quad (69)$$

i.e. exactly the same as in the quasi-static limit (25). So, the efficiency of the Otto cycle is independent of the driving speed. In particular, the efficiency does not depend on the power of the engine, what is totally different from the behaviour of the Carnot cycle discussed before. The constant efficiency does not mean, of course, that the heat and work are constant too. All energy flows go to zero when the driving speed grows, as shown in Fig. 9.

Fig. 10 shows a ST-diagram for an Otto cycle. In this diagram, one can also see the decrease of the work output per cycle for increasing speed, since the encircled area decreases. But in contrast to the Carnot cycle (Fig. 4), the finite speed causes spikes rather than loops.

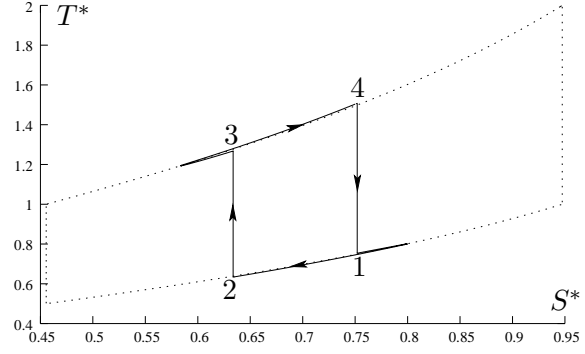


Fig. 10. ST-diagram for an Otto cycle of a four level system with $\{\epsilon_i\}_{i=1}^N = \{-3/2; -1/2; 1/2; 3/2\}$ and $\alpha_1 = 1, \alpha_2 = 2, \gamma_1 = 1, \gamma_2 = 2$. The dotted lines hold for the quasi-static limit, the solid lines for $\kappa T_R = 0.5$. The points 1 to 4 correspond to the respective points in Fig. 3.

6 Conclusions

We have considered a single quantum object with a discrete spectrum, an open system. The impact of its environment has been supposed to be reducible to a parametrized distortion of the spectrum and to a parametrized change of the occupation numbers. The internal energy U and the von Neumann entropy S can then be expressed as unique functions of these controls. The same holds for any pertinent thermodynamic quantity including those connected not just with a state, but with a process, i.e. heat and work. While there can be no operators underlying these quantities, they can, nevertheless, be defined for any appropriately embedded quantum system, even down to a single spin.

Thermodynamic machines arise, if a cycle is enforced on such a two-dimensional control space. The Carnot limit for their efficiencies has been proven and interpreted to result from the interplay between mechanical and statistical control rather than from the spectrum details or thermal equilibrium as such. Consequently, there is no way to violate the second law of thermodynamics, not even by using exotic attractor states.

While coherence has been excluded here, dynamical effects have been included after defining an internal relaxation time scale. The non-equilibrium features resulting from the finite control speed have been incorporated in terms of renormalized thermodynamic quantities. As has been shown, under such a non-quasi-static condition even the concept of a process temperature can still be applicable. Compared with the quasi-static one, this renormalized temperature turns out to be lower or higher, depending on the heat flow direction along the process.

The finite time heat and work exchange as well as the thermodynamic efficiency have been examined in detail, analytically and numerically, for two standard machine cycles: Carnot and Otto. Though there are some qualitative distinctions, both display rapid degradation of their machine function, when the driving speed is increasing. Contrary to the Carnot cycle, the Otto cycle’s efficiency remains speed-independent while energy flows decrease

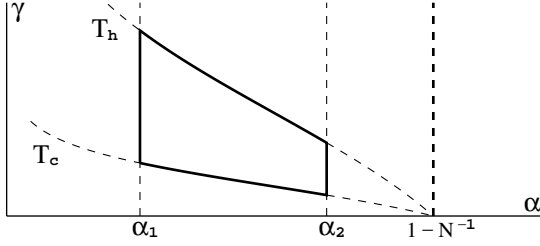


Fig. 11. Carnot cycle on the (α, γ) -plane associated with the nearly-uniform distribution (70) and $g(\gamma) = \gamma$. It is composed by segments of isentropes $\alpha = \alpha_{1,2}$ and isotherms $\gamma = T_{c,h} \cdot \Theta_U(\alpha)$ (72); ($T_h > T_c$).

up to zero. For the Carnot cycle the celebrated Curzon-Ahlborn result proves to be the lower bound for the efficiency at maximum power output.

We have as yet considered a special class of time dependence for the controls $\alpha(t)$ and $\gamma(t)$, namely, a linear one. Our approach is meant to be some kind of a minimal model capturing the essentials of any quantum thermodynamic machine deprived of coherence. Of course, this is not a substitute for investigations of particularized models; nonetheless, the approach presented allows one to treat any type of cycle under arbitrary dynamic regime on equal footing, putting aside, though, by which physical means this control might be implemented.

A Carnot cycle for non-canonical attractor

A.1 Nearly-uniform distribution

As a specific attractor consider the nearly-uniform distribution $\{\tilde{p}_i(\alpha)\}_{i=1}^N$:

$$\tilde{p}_i(\alpha) = \begin{cases} 1 - \alpha, & i = 1; \\ \alpha/(N - 1), & i = 2 \dots N. \end{cases} \quad \alpha \in (0, 1) \quad (70)$$

The temperature (8) in the quasi-static limit (2) can be written as

$$T = g(\gamma) \tilde{\epsilon} \ln^{-1} \frac{(N - 1)(1 - \alpha)}{\alpha}, \quad (71)$$

with $\tilde{\epsilon} := (N - 1)^{-1} \sum_{i=2}^N \epsilon_i - \epsilon_1$. From $\epsilon_1 < \epsilon_{(i>1)}$ it follows that $\tilde{\epsilon} > 0$, so the area of positive temperatures on the (α, γ) -plane is restricted by $\alpha < 1 - N^{-1}$.

The function Θ , that defines the shape of isothermal paths $g(\gamma) = T \cdot \Theta(\alpha)$, is now

$$\Theta_U(\alpha) = \tilde{\epsilon}^{-1} \ln \frac{(N - 1)(1 - \alpha)}{\alpha}; \quad (72)$$

and an example of the corresponding Carnot's cycle is sketched in Fig. 11.

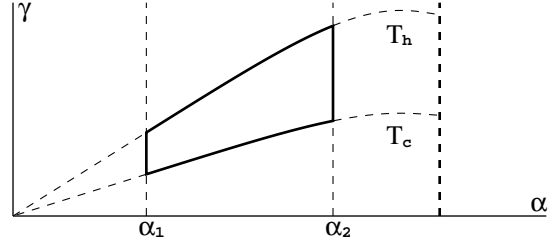


Fig. 12. Carnot cycle in the (α, γ) -plane associated with Tsallis' distribution (73) and $g(\gamma) = \gamma$ at $q = 1.4$ and $\{\epsilon_i\} = \{-3/2; -1/2; 1/2; 3/2\}$. The cycle is composed by segments of isentropes $\alpha = \alpha_{1,2}$ and isotherms $\gamma = T_{c,h} \cdot \Theta_{\mathcal{T}_s}(\alpha)$ (76); ($T_h > T_c$). Note that the domain of definition for (73) is restricted by $\alpha < [\max_i (q - 1)\epsilon_i]^{-1}$.

A.2 Tsallis' distribution

The attractor $\{\tilde{p}_i(\alpha)\}_{i=1}^N$ is now taken to be the Tsallis' distribution [28]:

$$\tilde{p}_i(\alpha) = Z_{\mathcal{T}_s}^{-1} \left(1 - \alpha(q - 1)\epsilon_i\right)^{\frac{1}{q-1}}, \quad (73)$$

$$Z_{\mathcal{T}_s} = \sum \left(1 - \alpha(q - 1)\epsilon_i\right)^{\frac{1}{q-1}};$$

with the specific parameter q , bounded by $q \in (0, 2)$; at $q = 1$ the case reduces to the canonical one (15).

Introducing the mean value $\langle \cdot \rangle$ and the covariance $\langle\langle \cdot; \cdot \rangle\rangle$ in a standard way:

$$\langle f \rangle := \sum f_i \tilde{p}_i, \quad \langle\langle f; g \rangle\rangle := \langle fg \rangle - \langle f \rangle \langle g \rangle, \quad (74)$$

as well as an auxiliary variable

$$u_i(\alpha; q) = \frac{\alpha(q - 1)\epsilon_i}{1 - \alpha(q - 1)\epsilon_i}, \quad (75)$$

one can now express the isotherm shape function $\Theta_{\mathcal{T}_s}(\alpha; q)$, resulting from (8), as

$$\Theta_{\mathcal{T}_s}(\alpha; q) = \alpha \frac{\langle\langle u; \ln(1 + u) \rangle\rangle}{\langle\langle u; u/(1 + u) \rangle\rangle}. \quad (76)$$

Note that $\ln(1 + u)$ and $u/(1 + u)$ are both increasing functions of u , therefore the RHS is always positive here.

An example of a Carnot cycle with isotherms of such a kind is sketched in Fig. 12. One can see that these isotherms are very similar to the canonical ones (cf. Fig. 1) as long as α is small enough. This is easily shown taking $\alpha\epsilon_i \ll 1$ for (76).

B Inequalities

Here we prove some inequalities concerning the heat and work flows in case of the canonical attractor $\{\tilde{p}_i(\alpha)\}_{i=1}^N$ (15). Considering the first derivative of $\tilde{p}_i(\alpha)$, one easily gets

$$\frac{d\tilde{p}_i(\alpha)}{d\alpha} = \sum_k (\epsilon_k - \epsilon_i) \tilde{p}_k(\alpha) \tilde{p}_i(\alpha) \quad (77)$$

and, consequently:

$$\begin{aligned} \sum_{i=1}^N \epsilon_i \frac{d\tilde{p}_i}{d\alpha} &= Z_{Can}^{-2} \sum_{i,k=1}^N \epsilon_i (\epsilon_k - \epsilon_i) e^{-\alpha(\epsilon_k + \epsilon_i)} \\ &= -Z_{Can}^{-2} \sum_{i < k} (\epsilon_k - \epsilon_i)^2 e^{-\alpha(\epsilon_k + \epsilon_i)} < 0. \end{aligned}$$

So, one gets

$$\sum \epsilon_i (d\tilde{p}_i/d\alpha) < 0, \quad (78)$$

that implies for $\alpha_1 < \alpha_2$ the following inequalities:

$$\sum \epsilon_i (\tilde{p}_i(\alpha_1) - \tilde{p}_i(\alpha_2)) > 0; \quad (79)$$

$$\sum \epsilon_i \int_{\alpha_1}^{\alpha_2} \alpha d\tilde{p}_i(\alpha) < 0. \quad (80)$$

Consider the terms $\sum \epsilon_i (p_i^{(1;2)} - \tilde{p}_i(\alpha_{1;2}))$ from (49), where the distributions $p_i^{(1;2)}$ at the cycle turning points are defined in (48). Integration by parts leads to:

$$\sum \epsilon_i (p_i^{(1;2)} - \tilde{p}_i(\alpha_{1;2})) = \pm \int_{\alpha_1}^{\alpha_2} \mathcal{F}_{1;2} \cdot \left(\sum \epsilon_i \frac{d\tilde{p}_i}{d\alpha} \right) \cdot d\alpha,$$

where

$$\mathcal{F}_{1;2} = \frac{\exp\{(\alpha - \alpha_{2;1})/\kappa\tau_R\} - \exp\{(\alpha_{2;1} - \alpha)/\lambda\kappa\tau_R\}}{\exp\{\mp\Delta\alpha/\kappa\tau_R\} - \exp\{\pm\Delta\alpha/\lambda\kappa\tau_R\}}.$$

Observing $\mathcal{F}_{1;2} > 0$ and (78), one comes up with:

$$\sum \epsilon_i (p_i^{(1;2)} - \tilde{p}_i(\alpha_{1;2})) \leq 0; \quad (81)$$

For the next inequality we need the following

Lemma: For any two monotone decreasing functions $f(x)$ and $h(x)$ the inequality $\int_a^b h(x)f(x)dx > 0$ follows from $\int_a^b h(x)dx = 0$.

Proof: Define $H(x) = \int_a^x h(x')dx'$ with the obvious property: $H(x) > H(a) = H(b) = 0$ for $a < x < b$. Applying integration by parts, one gets:

$$\begin{aligned} \int_a^b h(x)f(x)dx &= [H(x)f(x)]_a^b - \int_a^b \frac{df}{dx} H(x)dx \\ &= - \int_a^b \frac{df}{dx} H(x)dx > 0, \end{aligned}$$

observing $(df/dx) < 0$ and $H(x) > 0$.

Consider now the term $\sum \epsilon_i (p_i^{(2)} - p_i^{(1)})$ which occurs in RHS of (49) and (67). With (48) it reduces to

$$\begin{aligned} \sum \epsilon_i (p_i^{(2)} - p_i^{(1)}) &= \frac{1}{\kappa\tau_R} \left\{ 1 - e^{\frac{\Delta\alpha}{\kappa\tau_R} \frac{\lambda+1}{\lambda}} \right\}^{-1} \\ &\times \int_{\alpha_1}^{\alpha_2} h(\alpha) \left(\sum \epsilon_i \tilde{p}_i(\alpha) \right) d\alpha; \end{aligned} \quad (82)$$

with

$$h(\alpha) = e^{\frac{\alpha - \alpha_1}{\kappa\tau_R}} \left(1 - e^{\frac{\Delta\alpha}{\lambda\kappa\tau_R}} \right) + \frac{1}{\lambda} e^{\frac{\alpha_2 - \alpha}{\lambda\kappa\tau_R}} \left(e^{\frac{\Delta\alpha}{\kappa\tau_R}} - 1 \right).$$

One can easily check that both $\int_{\alpha_1}^{\alpha_2} h(\alpha)d\alpha = 0$ and $(dh/d\alpha) < 0$ hold. It follows from (78) that $\sum \epsilon_i \tilde{p}_i(\alpha)$ is a decreasing function of α as well. The lemma proven above ensures the integral in (82) to be positive and consequently:

$$\sum \epsilon_i (p_i^{(2)} - p_i^{(1)}) < 0. \quad (83)$$

Consider, at last, the term $\sum \epsilon_i \mathcal{I}_i$ from (55). The integral \mathcal{I}_i is defined in (53) and reduces to:

$$\int_{\alpha_1}^{\alpha_2} (\bar{p}_i - \tilde{p}_i(\alpha)) \alpha d\alpha = \left(\int_{\alpha_1}^{\bar{\alpha}} + \int_{\bar{\alpha}}^{\alpha_2} \right) (\bar{\alpha} - \alpha) \tilde{p}_i(\alpha) d\alpha,$$

where $\bar{\alpha} = (\alpha_2 + \alpha_1)/2$. It follows from the mean-value theorem that

$$\begin{aligned} \left(\int_{\alpha_1}^{\bar{\alpha}} + \int_{\bar{\alpha}}^{\alpha_2} \right) (\bar{\alpha} - \alpha) \left(\sum \epsilon_i \tilde{p}_i(\alpha) \right) d\alpha \\ = \sum \epsilon_i \tilde{p}_i(\theta_1) \int_{\alpha_1}^{\bar{\alpha}} (\bar{\alpha} - \alpha) d\alpha \\ + \sum \epsilon_i \tilde{p}_i(\theta_2) \int_{\bar{\alpha}}^{\alpha_2} (\bar{\alpha} - \alpha) d\alpha \\ = \sum \epsilon_i (\tilde{p}_i(\theta_1) - \tilde{p}_i(\theta_2)) \int_0^{\bar{\alpha}} u du, \end{aligned}$$

where $\alpha_1 < \theta_1 < \bar{\alpha} < \theta_2 < \alpha_2$. With (79) one gets:

$$\Delta\alpha \sum \epsilon_i \mathcal{I}_i = \sum \epsilon_i \int_{\alpha_1}^{\alpha_2} (\bar{p}_i - \tilde{p}_i(\alpha)) \alpha d\alpha > 0. \quad (84)$$

C Asymptotes

To get the asymptotic solution of the relaxation equation (37) in the slow driving limit $(v\tau_R/\Delta\alpha) \ll 1$, we start an iterative procedure: For this purpose we rewrite (37) as

$$p_i = \tilde{p}_i(\alpha) - v\tau_R (dp_i/d\alpha); \quad (85)$$

The zeroth approximation is given by $p_i \approx \tilde{p}_i(\alpha)$. The first order is obtained by the corresponding substitution on the right hand side of (85):

$$p_i \approx \tilde{p}_i - v\tau_R (d\tilde{p}_i/d\alpha). \quad (86)$$

This result, in turn, will be used, in the next iteration step:

$$p_i \approx \tilde{p}_i - v\tau_R (d\tilde{p}_i/d\alpha) + (v\tau_R)^2 (d^2\tilde{p}_i/d\alpha^2), \quad (87)$$

and so on.

Consider now the asymptotes for the distributions $p_i^{(1;2)}$ at the cycle's turning points (48), first, in the limit of very

slow driving, here $(\kappa\tau_R/\Delta\alpha) \ll 1$. Both $p_i^{(1)}$ and $p_i^{(2)}$ can be regarded as particular solutions of Eq. (85) obtained at the specially chosen parameters and initial values. So, $p_i^{(1)}$ is achieved at $\alpha = \alpha_1$ through the evolution with $v = -\lambda\kappa$ and $\alpha_0 = \alpha_2$ (47) started at $p_i^{(0)} = p_i^{(2)}$. With (87) one gets:

$$p_i^{(1)} = \tilde{p}_i(\alpha_1) + \lambda\kappa\tau_R \left(\frac{d\tilde{p}_i}{d\alpha} \right)_{\alpha_1} + o[\kappa\tau_R]; \quad (88)$$

Treating in the same way $p_i^{(2)}$, one comes up with:

$$p_i^{(2)} = \tilde{p}_i(\alpha_2) - \kappa\tau_R \left(\frac{d\tilde{p}_i}{d\alpha} \right)_{\alpha_2} + o[\kappa\tau_R]; \quad (89)$$

In the limit of very fast driving, $(\Delta\alpha/\kappa\tau_R) \ll 1$, one has to expand the exponents contained on the RHS of (48) into power series. Collecting terms up to first order in $\frac{\Delta\alpha}{\kappa\tau_R}$ yields the results for $p^{(1;2)}$ presented in Eq. (52). Their difference, $(p^{(2)} - p^{(1)})$, however, turns out to be of the second order and needs the adequate accuracy in the treatment.

D Proof for $Q_{12}^* < 0$

In the stationary cyclic regime the system state evolution on the low-temperature stage $1 \rightarrow 2$ is given by Eq. (38) taken with $v = \kappa$, $\alpha_0 = \alpha_1$ and $p_i^{(0)} = p_i^{(1)}$. Let us denote this particular solution of the relaxation equation (37) as p_i^* ; its boundary values prove to be $p_i^*(\alpha_{1;2}) = p_i^{(1;2)}$ from (48). Consider the derivative of the sum $\sum \epsilon_i p_i^*$ as a function $\varphi(\alpha)$:

$$\varphi(\alpha) := \frac{d}{d\alpha} \sum \epsilon_i p_i^* = -(\kappa\tau_R)^{-1} \sum \epsilon_i (p_i^* - \tilde{p}_i(\alpha)),$$

applying (37).

It follows from (81) that the boundary values of $\varphi(\alpha)$ turn out to be $\varphi(\alpha_{1;2}) \geq 0$, so there must be at least one $\alpha^* \in (\alpha_1; \alpha_2)$ such that $\varphi(\alpha^*) = 0$ and, consequently,

$$\sum \epsilon_i p_i^*(\alpha^*) = \sum \epsilon_i \tilde{p}_i(\alpha^*).$$

Choosing α^* as a new initial point for (38), one can employ this equality in order to recast $\sum \epsilon_i p_i^*$ and then $\varphi(\alpha)$ into the new form:

$$\begin{aligned} \sum \epsilon_i p_i^* &= \sum \epsilon_i \tilde{p}_i(\alpha^*) e^{-\frac{\alpha - \alpha^*}{\kappa\tau_R}} \\ &+ (\kappa\tau_R)^{-1} \int_{\alpha^*}^{\alpha} \left(\sum \epsilon_i \tilde{p}_i(\alpha') \right) e^{-\frac{\alpha - \alpha'}{\kappa\tau_R}} d\alpha' \\ &= \sum \epsilon_i \tilde{p}_i(\alpha) - \int_{\alpha^*}^{\alpha} e^{-\frac{\alpha - \alpha'}{\kappa\tau_R}} d \left(\sum \epsilon_i \tilde{p}_i \right); \\ \varphi(\alpha) &= (\kappa\tau_R)^{-1} \int_{\alpha^*}^{\alpha} e^{-\frac{\alpha - \alpha'}{\kappa\tau_R}} d \left(\sum \epsilon_i \tilde{p}_i \right). \end{aligned}$$

With (78) it is clear now that

$$\varphi(\alpha) \geq 0 \quad \text{for} \quad \alpha \leq \alpha^*, \quad (90)$$

so α^* introduced above is unique.

Consider now the integral originated from (32)

$$\int_{\alpha_1}^{\alpha_2} \alpha d \left(\sum \epsilon_i p_i^* \right) = \int_{\alpha_1}^{\alpha_2} \alpha \varphi(\alpha) d\alpha,$$

which yields the total heat exchange Q_{12}^* on the low-temperature isotherm $g(\gamma) = \alpha T_1$ of the Carnot cycle. It is convenient to split the interval of integration by α^* so that the mean-value theorem becomes employable:

$$\begin{aligned} \left(\int_{\alpha_1}^{\alpha^*} + \int_{\alpha^*}^{\alpha_2} \right) \alpha \varphi(\alpha) d\alpha &= \theta_1 \int_{\alpha_1}^{\alpha^*} \varphi(\alpha) d\alpha \\ &+ \theta_2 \int_{\alpha^*}^{\alpha_2} \varphi(\alpha) d\alpha, \end{aligned}$$

where $\alpha_1 < \theta_1 < \alpha^* < \theta_2 < \alpha_2$. According to (90), the first addend here is positive while the second one is negative. One estimates further:

$$\begin{aligned} &(\theta_1 \cdot \int_{\alpha_1}^{\alpha^*} + \theta_2 \cdot \int_{\alpha^*}^{\alpha_2}) \varphi(\alpha) d\alpha \\ &< \theta_2 \int_{\alpha_1}^{\alpha_2} \varphi(\alpha) d\alpha = \theta_2 \int_{\alpha_1}^{\alpha_2} d \left(\sum \epsilon_i p_i^* \right) \\ &= \theta_2 \sum \epsilon_i (p_i^{(2)} - p_i^{(1)}) < 0, \end{aligned}$$

as it follows from (83).

This completes the proof for

$$Q_{12}^* = \int_{\alpha_1}^{\alpha_2} \alpha d \left(\sum \epsilon_i p_i^* \right) < 0. \quad (91)$$

One of us (J. B.) gratefully acknowledges financial and other support from DAAD and the Russian Ministry for Education and Science in the framework of joint program ‘‘Michail Lomonosov’’. We thank Markus Henrich, Florian Rempp, and Georg Reuther for valuable discussions.

References

1. A. Bejan, *Advanced Engineering Thermodynamics* (Wiley, N.Y., 1988)
2. C. Truesdell, S. Bharatha, *Classical Thermodynamics as a Theory of Heat Engines* (Springer, New York, Berlin, 1977)
3. M. Toda, R. Kubo, N. Saito, *Statistical Physics I* (Springer Berlin, New York, 1983)
4. J. Gemmer, M. Michel, G. Mahler, *Quantum Thermodynamics* (Springer, 2004)
5. R.V. Chamberlain, *Science* **298**, 1172 (2002)
6. T.L. Hill, *Nano Letters* **1**, 111 (2001)
7. R. Alicki, *J. Phys. A* **12**, L 103 (1979)
8. T. Feldmann, R. Kosloff, *Phys. Rev. E* **68**, 016101 (2003)
9. E. Geva, R. Kosloff, *J. Chem. Phys.* **97**, 4398 (1992)
10. T. Jahnke, J. Birjukov, G. Mahler, *Eur. Phys. J. ST* (conference proceedings) **151**, 167 (2007)
11. M. Henrich, G. Mahler, M. Michel, *Phys. Rev. E* **75**, 051118 (2007)

12. M. Henrich, M. Michel, G. Mahler, *Europhys. Lett.* **76**, 1058 (2006)
13. J.P. Palao, R. Kosloff, J. Gordon, *Phys. Rev. E* **64**, 056130 (2001)
14. H.T. Quan, P. Zhang, C.P. Sun, *Phys. Rev. E* **73**, 036122 (2006)
15. H.E.D. Scovil, E.O. Schulz-Du Bois, *Phys. Rev. Lett.* **2**, 262 (1959)
16. D. Segal, A. Nitzan, *Phys. Rev. E* **73**, 026109 (2006)
17. F. Tonner, G. Mahler, *Phys. Rev. E* **72**, 066118 (2005)
18. L. Hackermüller, K. Hornberger, *Nature* **427**, 711 (2004)
19. F.L. Curzon, B. Ahlborn, *Am. J. Phys.* **43**, 22 (1975)
20. D.P. Sheehan, *AIP Conf. Proc.* (AIP Press, Melville, N.Y.) **643** (2002)
21. R. Jones, www.softmachines.org/wordpress/?p=127
22. T.P. Cheng, *Relativity, Gravitation and Cosmology* (Oxford U. P., 2005)
23. F. Rempp, M. Michel, G. Mahler, *Phys. Rev. A* **76**, 032325 (2007)
24. T.D. Kieu, *Phys. Rev. Lett.* **93**, 140403 (2004)
25. C.M. Bender, D.C. Brody, B.K. Meister, *Proc. Royal Soc. (London)* **A 458**, 1519 (2002)
26. C.V.d. Broeck, *Phys. Rev. Lett.* **95**(19), 190602 (2005)
27. Y. Izumida, K. Okuda, arXiv:0802.3759 (2008)
28. C. Tsallis, *J. Stat. Phys.* **52**, 169 (1988)